JOURNAL OF Materials CHEMISTRY

Continuous hydrothermal synthesis of inorganic materials in a near-critical water flow reactor; the one-step synthesis of nano-particulate $Ce_{1-x}Zr_xO_2$ ($x = 0$–1) solid solutions†

Albertina Cabañas,*[a] Jawwad A. Darr,[a]‡ Edward Lester[b] and Martyn Poliakoff*[a]

[a]*Clean Technology Research Group, School of Chemistry, The University of Nottingham, University Park, Nottingham, UK NG7 2RD*
[b]*School of Chemical, Environmental and Mining Engineering, The University of Nottingham, University Park, Nottingham, UK NG7 2RD*

Received 6th October 2000, Accepted 27th October 2000
First published as an Advance Article on the web 29th November 2000

$Ce_{1-x}Zr_xO_2$ solid solutions are produced continuously by hydrolysis of mixtures of cerium ammonium nitrate and zirconium acetate in near-critical water at *ca.* 300 °C and 25 MPa using a flow reactor. Rapid hydrothermal coprecipitation leads to nano-particulate $Ce_{1-x}Zr_xO_2$ ($x = 0$–1), the composition of which is largely determined by the initial relative concentrations of Ce^{4+} and Zr^{4+} ions in the starting solution. The freshly prepared materials are crystalline, possess very small particle sizes, and have high surface areas. The effects of calcining the products in air at high temperature have been studied. Apart from the 1 : 1 Ce : Zr solid solution, the phases of $Ce_{1-x}Zr_xO_2$ remain stable on calcining to 1000 °C, but the particles sinter and the surface areas decrease significantly. The materials have been characterised by Powder X-ray Diffraction (PXD), IR and Raman Spectroscopy, microanalysis, Thermogravimetric Analysis (TGA), X-ray Fluorescence (XRF) and BET (surface area measurements). In selected cases, high resolution Scanning Electron Microscopy (SEM) and Transmission Electron Microscopy (TEM) images were recorded to examine the particle morphology.

Introduction

The synthesis of ceria and ceria-containing materials is of considerable interest for applications as diverse as catalysts in car exhausts, glass polishing, ultraviolet absorbers, luminous materials, solid oxide fuel cells and ceramics.[1–5] $Ce_{1-x}Zr_xO_2$ solid solutions are widely used in three-way catalyst formulations for clean up of automotive gases.[1,6–11] Compared to CeO_2, $Ce_{1-x}Zr_xO_2$ shows improved ability to store and release oxygen (oxygen storage capacity, OSC) and greater thermal stability.[6] Furthermore, supported noble metal/ceria–zirconia catalysts have been also reported as having higher OSCs and can be reduced at significantly lower temperatures than CeO_2–ZrO_2 materials alone.[6]

Conventionally, solid solutions of $Ce_{1-x}Zr_xO_2$ can be prepared using methods such as high temperature solid state synthesis,[11,12] high energy ball milling,[9] sol–gel,[8,11] microemulsion methods[13] and co-precipitation with ageing of solutions.[14] However, many of these techniques are time consuming (multi-step syntheses or ageing), energy intensive and environmentally unfriendly. Additionally, when extremely small particle sizes are desired, the complexity, and sometimes the cost of manufacture, increases further. Here, we report a relatively simple procedure of preparing $Ce_{1-x}Zr_xO_2$ solid solutions using high temperature H_2O. Reactions in near critical (nc) and supercritical (sc) H_2O, so-called 'hydrothermal synthesis', have been carried out since the 19th century.[15] Metal oxides prepared using high temperature H_2O can be obtained in a highly crystalline state despite the relatively low temperatures often involved.[16–18] However, most of the published work has been carried out in batch reactors, with only limited control of the experimental conditions. For example, Hirano and Kato[19] recently reported the hydrothermal synthesis of $Ce_{1-x}Zr_xO_2$ solid solutions in a batch reactor, where solutions containing cerium(III) nitrate and zirconium oxychloride were co-precipitated with excess NH_3 and then subjected to hydrothermal conditions at 180 °C. However, a single phase was only obtained for $Ce_{0.12}Zr_{0.88}O_2$. In contrast to batch systems, flow reactors allow a better control of the experimental conditions. Arai and co-workers[20,21] have recently shown that nano- and micro-particulate pure CeO_2 and ZrO_2 can be produced continuously by decomposition of the corresponding metal nitrates in scH_2O. In a very recent Communication, we reported how $Ce_{1-x}Zr_xO_2$ solid solutions can be synthesised by hydrolysis of mixtures of $[NH_4]_2[Ce(NO_3)_6]$ (CAN) and $[Zr(ac)_4]$ in scH_2O, in the appropriate ratios.[22] The rapid hydrothermal co-precipitation technique permits the synthesis of nano-particulate $Ce_{1-x}Zr_xO_2$ solid solutions for the whole range of metal compositions ($x = 0$–1), the value of x being determined by the relative concentrations of CAN and $[Zr(ac)_4]$ in the precursor solution. In this paper, we study the thermal stability of the materials prepared in this way, by calcining the samples in air at 1000 °C. Full characterisation of both fresh and calcined materials is presented.

Experimental

Flow reactor

All experiments were conducted using a simple flow reactor built and designed in Nottingham.[22,23] The reactor, tubing and components were all made of 316 stainless steel (Swagelok). The apparatus (Fig. 1) consists of a metal salt solution pump, P (Gilson model 302/5.0 mL pump head), and a H_2O pump, P

†Electronic supplementary information (ESI) available: microanalysis results, FT-IR spectra. See http://www.rsc.org/suppdata/jm/b0/b008095k/

‡Present address: The IRC in Biomedical Materials, Queen Mary & Westfield College, University of London, Mile End Road, London, UK E1 4NS.

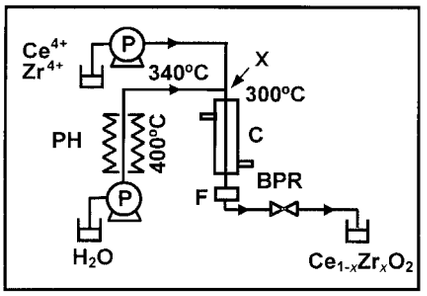

Fig. 1 Diagram of the flow reactor for the synthesis of metal oxide powders and solid solutions in $nc H_2O$. The parts are labelled as follows: (P) pump, (PH) pre-heater, (X) mixing point, (C) cooling, (F) filter, (BPR) back-pressure regulator. SAFETY: These experiments involve high pressures and high temperatures, they should therefore be approached with caution.

(Gilson model 303/10.0 mL pump head). H_2O was pumped through a pre-heating coil and heated to *ca.* 400 °C. It was then brought into contact with a concurrently flowing solution of metal salts at room temperature. Flow rates of 5 and 10 mL min^{-1} were used for the salt and water streams, respectively. At the mixing point (X in Fig. 1), the temperature was *ca.* 300 °C. The pressure was maintained at 25 MPa by a Dräger Tescom back-pressure regulator, BPR, Model 26-1700. Under these conditions, the residence time was less than 9 seconds, assuming that the density of the reaction mixture was the same as pure water[24] at the same temperature and pressure. The mixture was cooled immediately after the mixing point in the water cooler, C. The products were passed through a 7 μm filter, F, upstream of the BPR to remove any larger aggregates, and were then collected as aqueous suspensions. Solids were recovered by allowing the suspension to settle, decanting off the liquid phase and drying of the solid at *ca.* 100 °C. Suspensions with a high Zr content did not settle spontaneously and it was necessary to evaporate some water using a rotary evaporator. The damp solid was then dried at *ca.* 100 °C.

The enhanced self-dissociation constant of water under near-critical conditions[25] leads to rapid hydrolysis of the metal salts without addition of any base. The lower relative permittivity compared to room temperature[26] induces super-saturation and precipitation of metal hydroxide nanoparticles, which rapidly dehydrate to the corresponding oxide.

Materials

Cerium ammonium nitrate (CAN), $[NH_4]_2[Ce(NO_3)_6]$, and a zirconium acetate/dilute acetic acid solution (*ca.* 15% Zr) were used as obtained from Aldrich, without any special procedures to exclude air/moisture. All experiments were conducted using HPLC grade triply distilled water (BDH), which was not degassed.

0.21 M solutions of CAN and zirconium acetate were used to obtain pure CeO_2 and pure ZrO_2, respectively. For the $Ce_{1-x}Zr_xO_2$ solid solutions, the total concentration of metals in solution (Ce+Zr) was kept constant and equal to 0.21 M. Solutions were prepared containing mixtures of Ce and Zr salts at Ce : Zr ratios of 4 : 1, 1 : 1, 1 : 4 and 1 : 9.

Characterisation

Elemental analyses were performed at Nottingham by the Micro-Analytical Service (School of Chemistry). XRF information was obtained from a Spectro X-Lab 2000 Spectrometer using certified reference materials. XRF samples were made into glass disks melts in lithium tetraborate using an automatic fusion apparatus (Claisse Fluxy 30).

PXD data were collected using a Phillips XPERT θ–2θ diffractometer with Cu-Kα radiation. The sample was loaded onto an indented glass plate and scans were typically taken over a 2θ range of 20–80°. The PC IDENTIFY program was used to assess the purity of the ceria–zirconia powders by comparison to the JCPDS database. The APD program was used to estimate the size of the smallest particles in the sample by application of the Scherrer equation to the PXD line-widths (PC IDENTIFY and APD are part of the Phillips diffraction software package). For the calcined materials, the lattice parameters were obtained from the PXD by a standard least squares refinement.

Scanning Electron Microscope (SEM) images were obtained using a JEOL JSM-35C instrument. Samples were prepared by placing a small amount of sample on double-sided carbon tape, which was fixed onto an aluminium stub. The samples were coated with gold prior to analysis. Transmission Electron Micrograph (TEM) pictures were obtained using a JEOL JEM-2000FXII TEM operating at 200 KeV by placing one drop of a MeOH/powder suspension on a 3.05 mm diameter copper mesh (300 lines per inch mesh) and drying in air.

FT-Raman spectra were collected on a Perkin Elmer System 2000 spectrometer using a near-infrared source (1.064 μm), InGaAs detector with a laser power of between 200 and 800 mW for up to 300 scans. All standard FT-Raman samples were run in sealed high purity quartz capillaries. For most of the freshly prepared materials, the resolution of the FT-Raman spectra was poor and visible Raman spectra were therefore collected using a Renishaw RM 1000 Raman Microscope (Renishaw plc, Wotton-under-Edge, Gloucestershire, UK) using a 514 nm laser, Si CCD detector and motorised stage. Spectra were collected for at least 10 scans using a laser power of 5 mW. FTIR spectra were recorded for the powders as KBr disks on a Nicolet Avatar instrument.

Thermogravimetric Analysis (TGA) of the fresh materials was conducted in a Stanton Redcroft STA1000 instrument using the single pan arrangement. Approximately 100 mg of each sample was heated up to 600 °C under N_2 atmosphere at a heating rate of 10 °C min^{-1}. The N_2 flow rate around the sample cup was 50 mL min^{-1}.

Surface area measurements were made using a Micromeritics ASAP 2010 instrument using N_2 as the adsorptive gas. BET surface areas were calculated from the isotherm data using ASAP 2010 software. Prior to analysis, samples were degassed at 130 °C under vacuum for 8 hours to remove any residual moisture and other volatiles. Additionally, prior to the BET analysis, samples were subjected to purge and bake cycles to ensure reliable data were obtained.

Results and discussion

CeO_2, ZrO_2 and $Ce_{1-x}Zr_xO_2$ solid solutions were prepared as outlined in the Experimental section. Dry CeO_2 was obtained as a light yellow powder, whilst ZrO_2 was off-white. The solid solutions were yellow, becoming increasingly darker as the amount of Ce in the sample increased.

The effects of calcining the samples in air at high temperature were also studied. A sample of each material was heated in air using a tube furnace at 1000 °C for 1 h (excluding a 1 h period for the sample to cool to 200 °C in the furnace). Heat treatment causes the CeO_2 powder to change from light yellow to pale grey, whilst ZrO_2 remained off-white. The ceria–zirconia solid solutions were dark brown (4 : 1), dark yellow (1 : 1), yellow (1 : 4) and pale yellow (1 : 9) powders, respectively. To assess the stability of the calcined materials, samples were heated at 1000 °C for a further 3 h.

The materials were characterised by Powder X-ray Diffraction (PXD), IR and Raman spectroscopy, thermogravimetric analysis (TGA), microanalysis, X-ray Fluorescence (XRF) and BET (surface area measurements). For some samples, Scanning Electron Microscopy (SEM) and Transmission Electron Microscopy (TEM) images were obtained. The actual phase

Table 1 Ce : Zr molar ratio in the starting solutions and products (by XRF) for $Ce_{1-x}Zr_xO_2$ materials prepared in the near-critical flow reactor. Lattice type, particle size (PXD) and surface area, S_{BET}, for materials: fresh and calcined at 1000 °C for 1 h

Ce : Zr ratio		Fresh			Calcined at 1000 °C		
Starting solution	Product (XRF)	Lattice type	Size/ nm	S_{BET}/ $m^2\ g^{-1}$	Lattice type	Size/ nm	S_{BET}/ $m^2\ g^{-1}$
CeO_2	CeO_2	cubic	7	104(1)	cubic	145	1.7(1)
4 : 1	4 : 1.05	cubic	7	63.7(3)	cubic	17	6.6(1)
1 : 1	1 : 1.13	cubic	5 3–5[a]	107(1)	cubic	8 <15[a]	15.0(3)
1 : 4	1 : 4.21	tetragonal	4	181(3)	tetragonal	14	16.4(1)
1 : 9	1 : 8.48	tetragonal	4	184(4)	tetragonal	25	9.2(1)
ZrO_2	ZrO_2	monoclinic (40%) + tetragonal (60%)	6 5[a]	183(1)	monoclinic (80%) + tetragonal (20%)	27	11.4(1)

[a]By TEM.

assignment was made by a combination of PXD and Raman data. The results are summarised in Table 1.

Particle sizes for the solid solutions were estimated by applying the Scherrer equation to the line-widths of selected reflections. This gave a relatively narrow range of *ca.* 4–7 nm for the particles of the $Ce_xZr_{1-x}O_2$ solid solutions (see Table 1). After calcination at 1000 °C for 1 h, all of the materials sintered. Particle growth was particularly high for pure CeO_2, which, according to the Scherrer equation, reached 145 nm in size. For other materials, after calcining, particle sizes were between 8 and 27 nm.

We now discuss the information obtained from the different techniques in more detail.

X-Ray fluorescence (XRF)

Samples were analysed by XRF to determine the Ce to Zr ratio in the solid solutions. The results are shown in Table 1. Measured compositions were very close to those expected from the stoichiometry of the starting solutions. In most cases, however, the Zr content was slightly higher than expected.

Powder X-ray diffraction (PXD)

Fig. 2 shows PXD patterns of the $Ce_{1-x}Zr_xO_2$ solid solution ($x=0$–1) produced in the flow reactor. For the freshly prepared CeO_2 and $Ce_{1-x}Zr_xO_2$ solid solutions, a very broad PXD fluorite pattern was identified, as shown in Fig. 2a to e (top). As the concentration of the Zr in the solid solutions increases, the positions of the PXD peaks shift to greater 2θ values, indicating a decrease in the lattice parameter, caused by the incorporation of smaller Zr^{4+} ions into the ceria fluorite (mainly Ce^{4+}) lattice. The broadness of the reflections in the PXD pattern is associated with the small crystallite sizes. Yashima and colleagues[27] have reported that, when particle sizes of ceria–zirconia solid solutions are very small, line-broadening effects in the PXD pattern can make it difficult to differentiate between cubic and tetragonal lattices. However, they did find that ceria : zirconia solid solutions with a 1 : 4 ratio (which had been calcined up to 1590 °C) could be readily identified as tetragonal phase materials on the basis of their Raman spectra.[27] Thus, even though PXD suggested cubic-like phases for our fresh samples of $Ce_{1-x}Zr_xO_2$ solid solutions with $x=0.81$ and 0.90, tetragonal phases rather than cubic can be assigned on the basis of Raman spectra.

For pure ZrO_2, PXD data revealed a mixture of monoclinic (Baddelerite) and cubic-like phases (Fig. 2f). Under our reaction conditions (*ca.* 300 °C), the monoclinic phase (thermodynamic phase) is known to be strongly favoured for pure zirconia.[28] From the PXD pattern of ZrO_2, it was not clear whether the cubic-like phase was an unresolved tetragonal phase or a true cubic phase. It has been observed elsewhere[28] that very small crystallites can often stabilise a cubic form of zirconia (usually at room temperature). The Raman spectra of the material proved the tetragonality of the lattice (see discussion). Under flow reactor conditions, formation of the metastable tetragonal zirconia phase may be as a result of the rapid nature of the precipitation and relatively low synthesis temperature. By comparison of the intensities of the two most intense reflections in the respective PXD patterns, the ratio of monoclinic to tetragonal ZrO_2 was estimated to be 40 : 60.[29]

Fig. 2a to f (bottom) show PXD patterns of the different materials after calcining at 1000 °C for 1 h. Upon calcining the fresh CeO_2 sample, the cubic lattice was retained (PXD). However, the lines in the PXD pattern became sharper and the calculated particle size (using the Scherrer equation) increased to 145 nm (Table 1). PXD analysis of the calcined 4 : 1 material (Fig. 2b) showed a cubic lattice (with no splitting of any peaks). The calcined 1 : 1 material also suggested a cubic-like PXD pattern with some uneven peak shapes (Fig. 2c). For this material, the particles did not sinter very much during the

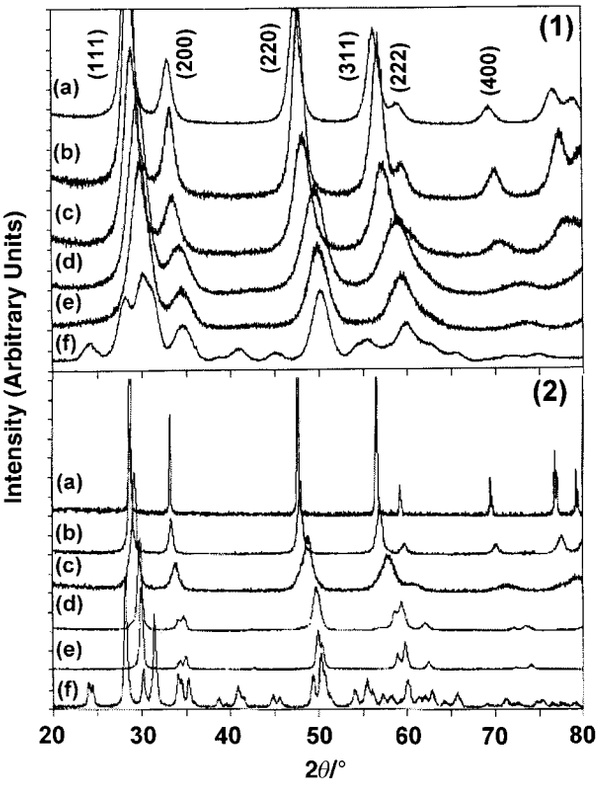

Fig. 2 Powder X-ray diffraction (PXD) patterns for $Ce_{1-x}Zr_xO_2$ materials (1) freshly prepared and (2) after calcining for 1 h at 1000 °C: (a) $x=0$ (pure CeO_2), (b) $x=0.21$, (c) $x=0.53$, (d) $x=0.81$, (e) $x=0.90$, (f) $x=1$ (pure ZrO_2).

thermal treatment. A tetragonal PXD pattern was suggested for the calcined 1 : 4 and 1 : 9 mixture, due to splitting of the (200), (220), (311) and (400) peaks to give new (002), (202), (113) and (004) reflections, respectively (Fig. 2d and e). Peak splittings of the PXD pattern of the calcined 1 : 9 material were clearer than those of the calcined 1 : 4 material. As a consequence of the calcining treatment, the tetragonal or pseudo-cubic metastable phase of ZrO_2 partially transformed to the stable monoclinic phase and only small amounts of the tetragonal phase were retained (Fig. 2f). The ratio of monoclinic to tetragonal phases changed to 80 : 20.

Further calcination of the samples at 1000 °C for 3 h did not affect the $Ce_{1-x}Zr_xO_2$ solid solutions substantially except for the 1 : 1 mixture. With longer heating, this sample apparently separated into a large range of solid solutions of different compositions, not resolved in the PXD. The uneven shape of the PXD peaks of the 1 : 1 material calcined for 1 h probably indicates an incipient phase separation.

Comparison of the PXD pattern of the calcined $Ce_{1-x}Zr_xO_2$ solid solutions to the JCPDS database gave a reasonably good match for some of the compositions. Cubic patterns corresponding to $Ce_{0.75}Zr_{0.25}O_2$ and $Ce_{0.60}Zr_{0.40}O_2$ [file numbers 28-0271 and 38-1439, respectively] and tetragonal patterns for $Ce_{0.5}Zr_{0.5}O_2$ and $Ce_{0.16}Zr_{0.84}O_2$ [file numbers 38-1436 and 38-1437, respectively] were compared with the calcined $Ce_{1-x}Zr_xO_2$ solid solutions with $x = 0.21$, 0.53, 0.81 and 0.90. Minor shifts of the reflections are consistent with the slight differences in the composition.

For the $Ce_{1-x}Zr_xO_2$ solid solutions calcined for 1 h, the lattice parameters were obtained from the PXD line positions of the different reflections using a least square refinement method. Table 2 shows the lattice parameters a (cubic phase), a and c (tetragonal phase) or a, b, c and β (monoclinic phase) obtained from the refinement according to the phase assignment shown in Table 1. For the calcined ZrO_2, only the lattice parameters of the monoclinic phase were refined due to the overlapping of the few identifiable tetragonal peaks with some of the monoclinic ones as well as the lower intensity of the tetragonal peaks. For the fresh materials no attempt at refinement was made due to the broadness of some peaks which was responsible for the unresolved splitting of the tetragonal phases and the overlapping of the monoclinic and tetragonal phases in the PXD pattern.

Fig. 3 shows the relationship between the lattice parameters of CeO_2 and $Ce_{1-x}Zr_xO_2$ solid solutions after calcining and the percentage of Zr in the sample. As the Zr content of the solid solution increases, the lattice parameters decrease. The tetragonal distortion is a lengthening of the c axis.

After calcining, the lattice parameters for cubic phases (a) are slightly shorter than those reported in the JCPDS database for $Ce_{1-x}Zr_xO_2$ solid solutions with $x = 0.25$ and 0.4. The differences may be due to the different synthetic routes. Ceria-containing materials have highly defective structures. The slightly shorter lattice parameter found in our materials after calcining may indicate a higher number of oxygen vacancies in the structure. Besides, larger uncertainties are

Table 2 Lattice parameters a (cubic), a and c (tetragonal) or a, b, c and β (monoclinic) obtained by refining the PXD pattern of the calcined $Ce_{1-x}Zr_xO_2$ solid solutions

Ce : Zr ratio	a/Å	c/Å	n^b
CeO_2	5.4115(2)	—	7
4 : 1	5.351(6)	—	5
1 : 1	5.26(1)	—	6
1 : 4	5.153(4)	5.245(4)	11
1 : 9	5.116(3)	5.217(4)	11
ZrO_2[a]	5.17(1)	5.34(1)	27

[a]For the monoclinic cell $b = 5.22(1)$ and $\beta = 99.4(1)$ °. [b]Number of peaks included in the refinement.

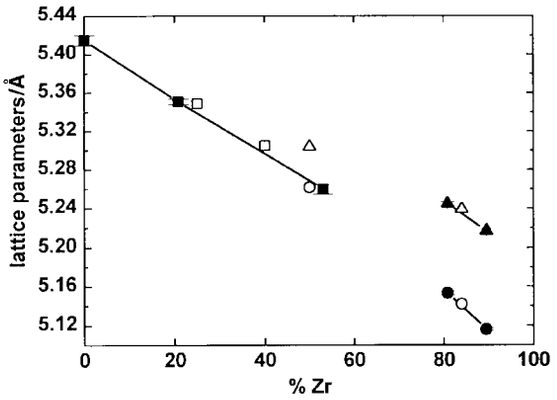

Fig. 3 Lattice parameters against molar Zr content (%) of calcined $Ce_{1-x}Zr_xO_2$ solid solutions: (■) a cubic; (●) a tetragonal; (▲) c tetragonal, compared with bibliographic (JCPDS): (□) a cubic; (○) a tetragonal; (△) c tetragonal. The solid lines connecting the lattice parameters of the calcined $Ce_{1-x}Zr_xO_2$ are drawn as a visual aid.

expected in the refinement of the cell parameters in the cubic system. The lattice parameters of the tetragonal $Ce_{0.16}Zr_{0.84}O_2$ phase reported in the JCPDS database match very well with those found in this work. A less good match was found between our $Ce_{0.47}Zr_{0.53}O_2$ material and the $Ce_{0.5}Zr_{0.5}O_2$ pattern from the literature. For this composition, the PXD pattern of the material reported in the JCPDS database is tetragonal and corresponds to a metastable phase made by "non-equilibrium" cooling conditions. In our work, however, beside the irregular form of the peaks in the PXD pattern of the 1 : 1 mixture, indexing was made on the basis of a cubic or pseudo-cubic phase. As suggested before, partial demixing in the 1 : 1 material calcined for 1 h could explain these differences.

Raman spectroscopy

Raman spectra of the fresh and calcined samples were collected over the range 200–700 cm^{-1} in order to assign the actual phases of the different solid solutions. For the freshly prepared materials apart from pure CeO_2, Raman spectra were collected using a Raman microscope. After calcining at 1000 °C for 1 h, the materials gave generally stronger and better-defined Raman shifts, probably as a result of the higher degree of crystallinity. In these cases, sufficient resolution could be achieved with the FT-Raman. For the calcined ZrO_2 sample, however, Raman spectra were still collected with the Raman microscope.

Raman spectra of fresh and calcined $Ce_{1-x}Zr_xO_2$ solid solutions are shown in Fig. 4 and 5. All Raman spectra of the freshly prepared pure ceria and the ceria–zirconia solid solutions with high cerium content (Ce : Zr ratios 4 : 1 and 1 : 1) showed a single very broad strong peak at 461, 465 and 463 cm^{-1}, respectively, due to the T_{2g} Raman active mode of a cubic fluorite structure.[28,30] A shoulder at *ca.* 610 cm^{-1} was also observed for the 4 : 1 and 1 : 1 Ce : Zr solid solutions, which can be attributed to the presence of oxygen vacancies in ceria-containing materials.[28,31]

Raman spectra for the fresh 1 : 4 and 1 : 9 materials were similar with broad bands at *ca.* 625, 460 and 315 cm^{-1}, respectively. For the fresh 1 : 9 material, another weak peak at 278 cm^{-1} was also observed. Hence, the Raman spectra of these materials suggest the possible presence of unresolved tetragonal materials[1,27,28,30,32,33] (*i.e.* not all the peaks are resolved due to the broadness of the bands). On this basis, the fresh 1 : 4 and 1 : 9 materials were assigned as tetragonal phases rather than cubic as was suggested from their broad PXD patterns.

A complex spectrum with up to 12 bands in the range analysed was collected for the fresh ZrO_2. The appearance of so many bands is indicative of monoclinic ZrO_2.[30] For the

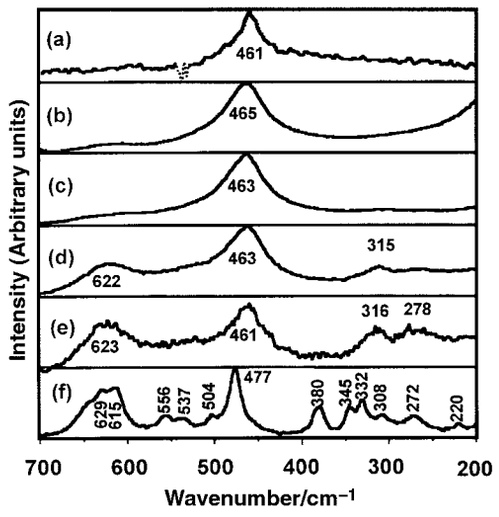

Fig. 4 Raman spectra for $Ce_{1-x}Zr_xO_2$ materials prepared in the near-critical water flow reactor: (a) $x=0$ (pure CeO_2), (b) $x=0.21$, (c) $x=0.53$, (d) $x=0.81$, (e) $x=0.90$, (f) $x=1$ (pure ZrO_2). The spectrum of pure CeO_2 was collected with the FT-Raman and shows an artefact at 535 cm^{-1} due to the quartz tube (dotted line).

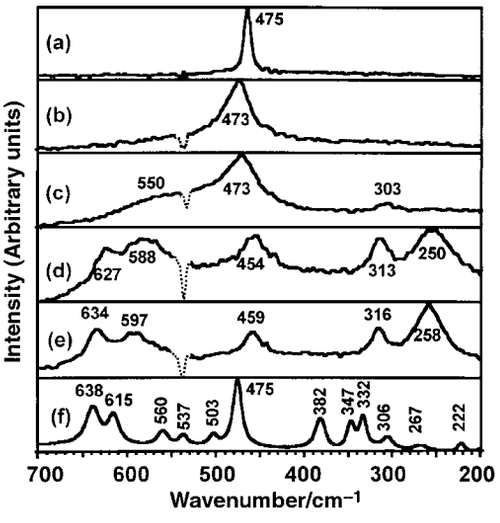

Fig. 5 Raman spectra for $Ce_{1-x}Zr_xO_2$ materials calcined at 1000 °C for 1 h: (a) $x=0$ (pure CeO_2), (b) $x=0.21$, (c) $x=0.53$, (d) $x=0.81$, (e) $x=0.90$, (f) $x=1$ (pure ZrO_2). The artefact at 535 cm^{-1} for (a) to (e) is due to the quartz tube (dotted line).

monoclinic phase, up to 18 vibration modes are expected to be Raman active.[34] Peaks attributed to tetragonal and monoclinic phases tend to overlap in the Raman spectrum.

After calcining, the pure CeO_2 sample showed a single strong sharp peak at 475 cm^{-1} due to the T_{2g} Raman active mode of the cubic fluorite structure. Similarly, the spectrum of the calcined $Ce_{1-x}Zr_xO_2$ solid solutions with a Ce : Zr ratio of 4 : 1 resembled that of pure CeO_2, but with a broader peak, now at 473 cm^{-1}. The broadening of this peak may be related to the partial substitution in the lattice of Ce^{4+} by Zr^{4+} cations. For the calcined Ce : Zr 1 : 1 material, the strongest band at 473 cm^{-1} showed a very broad shoulder at *ca.* 580 cm^{-1} (associated with oxygen vacancies[28,31]) and additional weak peaks at lower wavenumbers (such as one at 303 cm^{-1}) that could suggest tetragonalization of the lattice[33] but could also be as a result of the incipient phase separation. For cell refinement purposes, however, a cubic phase was chosen.

The calcined 1 : 4 and 1 : 9 samples showed at least five peaks between 200 and 700 cm^{-1}. These results are consistent with the expected six Raman active bands of a tetragonal phase reported in the literature.[1,27,28,30,32,33,34] We were unable to observe the expected weak band at *ca.* 150 cm^{-1} because it was outside the instrument range. After calcining, pure ZrO_2 showed a complex pattern with weak intensity scattering, very similar to that found in the fresh ZrO_2. Up to 12 peaks were resolved and could be assigned to a mixture of monoclinic and tetragonal phase(s) of ZrO_2 [1,34] as suggested by the PXD pattern.

Table 3 Expected phases for the $Ce_{1-x}Zr_xO_2$ solid solutions (modified from ref. 28)

Phase	$Ce_{1-x}Zr_xO_2$	*c*/*a*	Space group
monoclinic (m)	$x>0.8$	—	$P2_1/c$
tetragonal (t)	$0.8>x>0.6$	>1	$P4_2/nmc$
tetragonal (t′)	$0.6>x>0.35$	>1	$P4_2/nmc$
tetragonal (t″)	$0.35>x>0.2$	1	$P4_2/nmc$
cubic (c)	$x<0.2$	1	$Fm3m$

The structural phase transitions of the system Ce–Zr–O have been extensively studied by Yoshimura and co-workers.[12,27,35,36] and are summarised in Table 3 (modified from ref. 28). Three possible structures: monoclinic, tetragonal and cubic, have been identified in the literature $Ce_{1-x}Zr_xO_2$ solid solutions[28] depending on the composition. Furthermore, there are several stable and metastable phases having tetragonal symmetry. At high CeO_2 concentration ($x<0.2$), $Ce_{1-x}Zr_xO_2$ crystallises in a fluorite-type structure, whereas for pure ZrO_2 and ZrO_2-rich solid solutions ($x>0.8$) monoclinic phases are observed. At lower Zr content ($0.8<x<0.2$) three different tetragonal phases (namely t, t′ and t″) have been distinguished in the literature: t, the stable phase, formed through a diffusion phase decomposition; t′, a metastable phase obtained through a diffusionless transition and t″, an intermediate between t′ and c. In t″, the cation sublattice is cubic but there is a displacement of the O atoms from their ideal fluorite sites.[28]

The precise phase assignment found in this paper (Table 1) is slightly different from that reported in the literature[35] (Table 3). For the fresh and calcined 1 : 9 mixture, we have found a tetragonal rather than a monoclinic phase. For the fresh $Ce_{1-x}Zr_xO_2$ solid solutions with $x=0.53$, we have found a cubic pseudo-fluorite instead of a tetragonal structure. After calcining this material at 1000 °C for 1 h, either a partial tetragonalization of the lattice or some phase segregation has been observed in the Raman spectrum. The different phase assignment, however, may arise because previous samples[35] were treated at much higher temperatures than samples in this work.

Scanning and transmission electron microscopy (SEM and TEM)

SEM images were recorded for pure CeO_2 at ×4700 magnification, showing particles that were less than 0.1 μm diameter (100 nm) but not well resolved (not shown here).

TEM images of the fresh 1 : 1 mixture (*i.e.* $Ce_{0.47}Zr_{0.53}O_2$) showed particles of similar size to the estimates made from the PXD data. Fig. 6 shows particles of less than 10 nm with well-defined edges, which were either separated or in loose clumps.

Fig. 7 shows the approximate particle size distribution for the sample in Fig. 6, estimated by measuring the length of the largest axis of each particle for a sample of 225 particles. The histogram suggests a relatively narrow particle size distribution with effectively 88% of the particles between 3 and 5 nm.

Particle sizes of the calcined solid solutions were estimated (by PXD) to be in the 8–25 nm range (Table 1). The PXD data for the 1 : 1 calcined sample suggested that the particle size had increased from 5 to only 8 nm. Particles of the solid solutions with lowest and highest Zr contents grow much larger after calcining, whilst particles from the 1 : 1 mixture are affected the least. A TEM study of the calcined 1 : 1 solid solution revealed higher primary particles than those estimated by PXD, of *ca.*

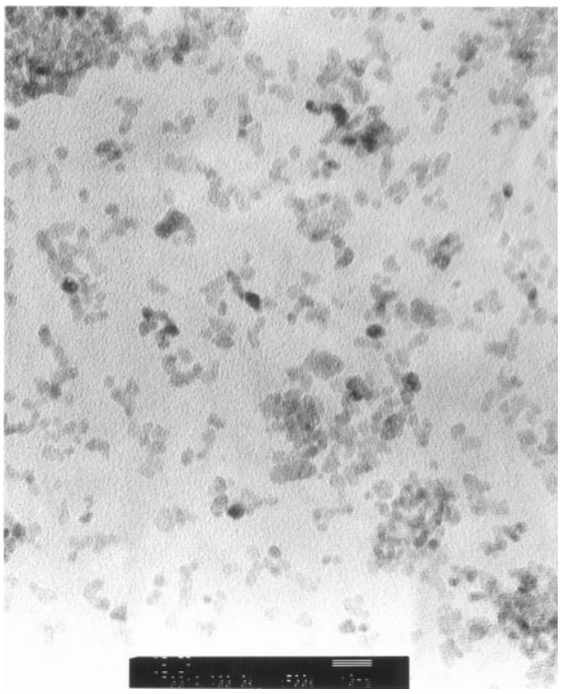

Fig. 6 Transmission electron micrograph (TEM) of $Ce_{0.47}Zr_{0.53}O_2$ synthesised in the flow reactor (bar = 10 nm).

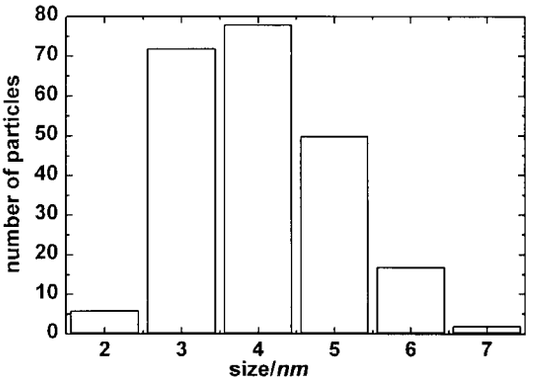

Fig. 7 Histogram for the 1 : 1 Ce : Zr mixture showing the particle size distribution of sample in Fig. 6 (based on 225 particles).

15 nm in diameter which appear to be tightly bunched into large dense aggregates (Fig. 8).

The smallest particles in the fresh ZrO_2 sample were estimated to be *ca.* 7 nm using the Scherrer equation (Table 1). This value gives good correlation with the primary particle size of the ZrO_2 observed in the TEM (Fig. 9). The TEM images revealed aggregates of primary particles (*ca.* 5 nm) arranged in fluffy 'cloud-like' structures. The particles did not appear to have well-defined edges.

For the 1 : 1 Ce : Zr solid solution, the electron diffraction patterns obtained from the TEM consisted of a number of concentric rings, which confirmed the crystallinity of the materials. Owing to the random alignment of the crystallites and, hence, of the different lattice planes in the lattice with respect to the electron beam, when the beam is diffracted it forms a cone around the original direction. For pure ZrO_2, electron diffraction patterns showed very weak rings suggesting poorer crystallinity.

Microanalyses

Microanalytical C, H and N data for the fresh materials are deposited as electronic supplementary information.† As suspected, some of the materials show significant C and N

Fig. 8 Transmission electron micrograph (TEM) of $Ce_{0.47}Zr_{0.53}O_2$ after calcining at 1000 °C for 1 hour (bar = 20 nm).

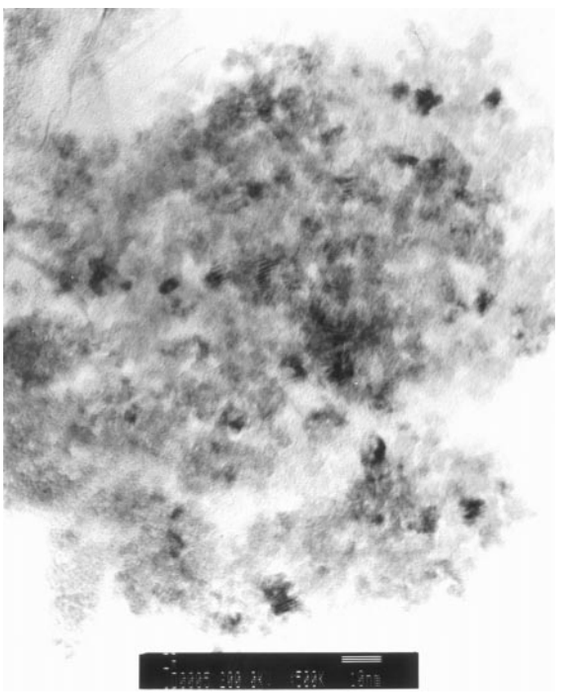

Fig. 9 Transmission electron micrograph (TEM) of ZrO_2 synthesised in the flow reactor (bar = 10 nm).

incorporation (up to 2.17% C for ZrO_2 and 4.69% N for CeO_2). This is not surprising since they were prepared from precursors which contain significant amounts of C or N. The particles contain either acetate or nitrate (or ammonia) ligands on their surfaces. The C and N content in the samples correlates with the C and N content of the starting solutions. Upon calcining, the anionic ligands are removed from the surface as expected, and the microanalyses showed no C and N in the materials.

Infra-red spectroscopy

FTIR spectra were collected between 400 and 4000 cm^{-1} for the fresh and calcined samples and, in agreement with the

microanalytical data, there appeared to be significant peaks due to coordinated acetate anions and nitrogen-containing groups (nitrate and ammonia ions) in the fresh materials.[37] FTIR spectra of $Ce_{1-x}Zr_xO_2$ solid solutions in the range 400–1800 cm^{-1} are also deposited as electronic supplementary information.† All the samples contain a considerable amount of water (bending mode of water appears at *ca.* 1630 cm^{-1}). In pure ZrO_2 and $Ce_{1-x}Zr_xO_2$ solid solutions, peaks between 1550 and 1340 cm^{-1} confirm the presence of acetate ions on the surface. In pure CeO_2 and $Ce_{1-x}Zr_xO_2$ solid solutions, a very sharp and intense peak centred at 1384 cm^{-1} and two weak broad bands at *ca.* 1500 and 1320 cm^{-1} indicated the presence of nitrate groups. An intense and very broad band centred at *ca.* 3400 cm^{-1} confirmed the presence of water in all the samples. A shoulder on this peak between 3200 and 3100 cm^{-1} suggested the presence of ammonia groups in pure CeO_2. As a consequence of the different Ce- and Zr-containing precursors, peaks due to acetate were stronger in the materials with a high Zr content (as zirconium acetate is the precursor) and peaks due to nitrate were strongest for the materials containing a high Ce content. Metal oxide stretches appeared unresolved as a broad and intense band between 400 and 700 cm^{-1}.

After the calcining procedure, the IR spectra showed no trace of either acetate or nitrate and are, thus, in concordance with the microanalytical data.

Thermogravimetric analyses (TGA)

Thermogravimetric analysis was performed on the fresh samples. Each sample was heated in N_2 from room temperature to 600 °C, at a rate of 10 °C min^{-1}. TGA data for the fresh samples are shown in Fig. 10. In each case, there was a detectable weight loss (2–12)% below 120 °C, presumably due to adsorbed water. Some samples showed small weight losses (4–7)% in the ranges 250–270 °C and from *ca.* 300 °C. IR spectra suggest that these losses are associated with residual nitrate and acetate groups, respectively. In the literature, differential thermal analysis of zirconium acetate showed that crystallisation of zirconia occurs along with pyrolytic breakdown of the acetate groups at *ca.* 370 °C.[38] Any weight lost at slightly lower temperatures (from *ca.* 300 °C) may reflect the weaker bond energy of the acetate groups attached to the surface of the products. In our work, the decomposition of nitrate groups seems to occur between 250 and 270 °C. However, peaks overlap reflecting the simultaneous loss of acetate and nitrate groups at certain temperatures.

BET data

BET data were run as described in the Experimental section. In all cases, the samples were dried at 130 °C prior to analyses under vacuum. This resulted in a weight loss of several percent for some of the materials, believed to be loss of water, roughly equating to the initial weight loss seen during TGA analysis. The isotherms were clearly "Type II" corresponding to non-porous particles for the fresh and calcined ceria and solid solution powders. A full adsorption/desorption program was run between 0 and 1 relative pressures to confirm the absence of any mesopores. This was carried out on a selection of different samples. In each case, the desorption trace demonstrated the absence of any mesopores in the sample structure.

Surface areas, S_{BET}, are shown in Table 1 for both fresh and calcined materials. Fig. 11 shows S_{BET} for the CeO_2, ZrO_2 and solid solutions *versus* the % molar Zr in the sample; freshly prepared (top) and calcined at 1000 °C for 1 h (bottom). Additionally in Fig. 11, the variation of particle size (PXD) with composition is also represented.

S_{BET} values for the fresh samples appeared to reach a maximum for the 1 : 4 and 1 : 9 Ce : Zr materials (181 and 184 $m^2\,g^{-1}$, respectively), as well as for pure ZrO_2 (183 $m^2\,g^{-1}$). The plot suggests that there is a strong correlation between the calculated particle size (by PXD) and the S_{BET} values. The higher surface areas of the 1 : 4 and 1 : 9 materials are due to the very small size of the particles.

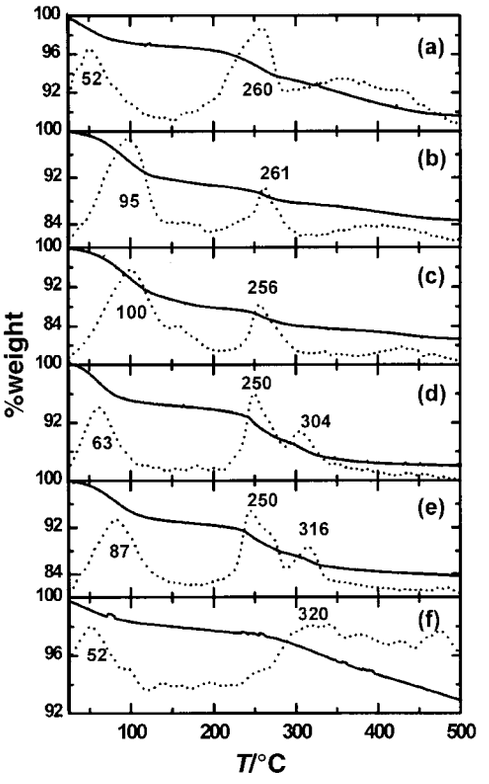

Fig. 10 TGA data for $Ce_{1-x}Zr_xO_2$ materials prepared in the near-critical water flow reactor: (a) $x=0$ (pure CeO_2), (b) $x=0.21$, (c) $x=0.53$, (d) $x=0.81$, (e) $x=0.90$, (f) $x=1$ (pure ZrO_2). The solid lines show the weight loss *versus* temperature and dotted lines are the first derivatives of the solid lines.

After the calcining treatment, surface areas decrease considerably as expected with S_{BET} lower than 17 $m^2\,g^{-1}$ (maximum value found for the 1 : 4 Ce : Zr mixture). For the

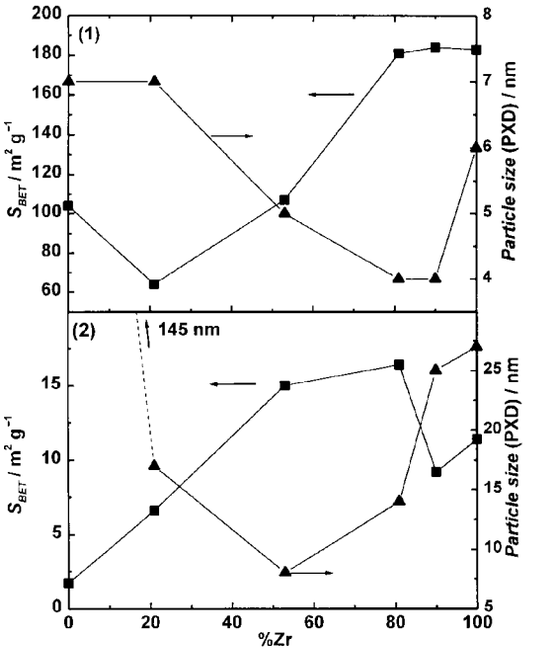

Fig. 11 S_{BET} area measurements (■) and estimated particle sizes by PXD (▲) of $Ce_{1-x}Z_xO_2$ solid solutions (1) freshly prepared and (2) after calcining for 1 h at 1000 °C against molar Zr content (%).

1 : 1 Ce : Zr solid solution, surface area is 15 $m^2 g^{-1}$. Pure CeO_2 particles sinter very easily and the crystallite size reaches 145 $m^2 g^{-1}$ with a low surface area of 1.7 $m^2 g^{-1}$.

Conclusions

We have reported a novel and extremely rapid one-step method for the synthesis of ceria–zirconia solid solutions. The chemistry is clean and extremely simple. The reaction does not require the addition of a modifier (to control pH) or prolonged reaction times. In principle, any composition of $Ce_{1-x}Zr_xO_2$ should be accessible by simply varying the amounts of precursors in the starting solution. The products are completely homogenous, in contrast to materials produced by techniques such as sol–gel, co-precipitation or ball milling. In selected cases, the particles are highly crystalline despite the relatively low temperatures of formation, and the primary particle sizes are extremely small imparting relatively high surface areas of up to *ca.* 190 $m^2 g^{-1}$ for these materials.

We have been able to show that most of the freshly precipitated solid solutions appear to have cubic or pseudo-cubic structures based on their PXD patterns. Raman studies have been useful in identifying the actual phase(s) present in the materials with a high degree of certainty, which is not always possible using PXD data alone. PXD peaks for the calcined samples become sharper and the particles grow larger as a result of calcining treatment.

Acknowledgements

We acknowledge the financial support of the TMR research network Superclean Chemistry-2 Contract No. ERBFMRXCT970104, EPSRC Grant No. GR/N06892 and ICI. We thank N. Bock (SEM and TEM pictures), T. R. Spencer (Microanalyses), M. Guyler and K. Stanley for technical support and Dr D. A. Graham, Dr P. A. Hamley and S. J. Barlow, for their assistance and discussions. Renishaw Ltd. are thanked for use of the Raman microscope.

References

1 A. Trovarelli, *Catal. Rev*, 1996, **38**, 439.
2 T. Masui, K. Fujiwara, K. Machida and G. Adachi, *Chem. Mater.*, 1997, **9**, 2197.
3 W. Chengyun, Q. Yitai, X. Yi, W. Changsui, Y. Li and Z. Guiwen, *Mater. Sci. Eng. B*, 1996, **39**, 160.
4 B. C. H. Steele, *Ceram. Int.*, 1993, **19**, 269.
5 S. H. Oh and C. C. Eickel, *J. Catal.*, 1998, **112**, 543.
6 G. Vlaic, R. DiMonte, P. Fornasiero, E. Fonda, J. Kaspar and M. Graziani, *Stud. Surf. Sci. Catal.*, 1998, **116**, 185.
7 T. Sato, Y. Inoue, T. Odashima, M. Ishitsuka and E. Min, *Br. Ceram. Trans.*, 1996, **95**, 99.
8 A. Deptula, M. Carewska, T. Olczak, W. Lada and F. Croce, *J. Electrochem. Soc.*, 1993, **140**, 2294.
9 C. de Leitenberg, A. Trovarelli, F. Zamar, G. Maschio, G. Dolcetti and J. Llorca, *J. Chem. Soc., Chem. Commun.*, 1995, 2181.
10 M. Ozawa, M. Kimura, H. Sobukawa and K. Yokota, *Toyota Tech. Rev.*, 1992, **27**, 43.
11 T. Masui, Y. Peng, K. Machida and G. Adachi, *Chem. Mater.*, 1992, **10**, 4005 and references therein.
12 M. Yashima, K. Morimoto, N. Ishizawa and M. Yoshimura, *J. Am. Ceram. Soc.*, 1993, **76**, 1745.
13 T. Masui, K. Fujiwara, Y. Peng, T. Sakata, K. Machida, H. Mori and G. Adachi, *J. Alloys Compd.*, 1998, **269**, 116.
14 B. Djurcic, D. McGarry and S. Pickering, *J. Mater. Sci. Lett.*, 1993, **12**, 1320.
15 A. Rabenau, *Angew. Chem., Int. Ed. Engl.*, 1985, **24**, 1026.
16 J. A. Darr and M. Poliakoff, *Chem. Rev.*, 1999, **99**, 45.
17 J. A. Darr and M. Poliakoff, *Abstr. Pap. Am. Chem. Soc.*, 1998, **216**, 224.
18 A. Cabanas, J. A. Darr, T. Ilkenhans and M. Poliakoff, in the *Proceedings of the 6th Meeting on Supercritical Fluids*, eds.M. Poliakoff, M. W. George and S. M. Howdle, International Society for the Advancement of Supercritical Fluids, Nancy, 1999.
19 M. Hirano and E. Kato, *J. Ceram. Soc. Jpn*, 1996, **104**, 958.
20 T. Adschiri, K. Kanazawa and K. Arai, *J. Am. Ceram. Soc.*, 1992, **75**, 1019.
21 Y. Hakuta, S. Onai, S. Terayama, T. Adschiri and K. Arai, *J. Mater. Sci. Lett.*, 1998, **17**, 1211.
22 A. Cabanas, J. A. Darr, E. Lester and M. Poliakoff, *Chem. Commun.*, 2000, 901.
23 A. A. Galkin, B. G. Kostyuk, V. V. Lunnin and M. Poliakoff, *Angew. Chem.*, 2000, **39**, 2738.
24 E. Schmidt, *Properties of Water and Steam in SI-Units*, Springer-Verlag, Berlin, 1969.
25 W. L. Marshall and E. U. Franck, *J. Phys. Chem. Ref. Data*, 1981, **10**, 295.
26 M. Uematsu and E. U. Franck, *J. Phys. Chem. Ref. Data*, 1980, **9**, 1291.
27 M. Yashima, K. Ohtake, M. Kakihana and M. Yoshimura, *J. Am. Ceram. Soc.*, 1994, **77**, 2773.
28 P. Fornasiero, G. Balducci, R. DiMonte, J. Kaspar, V. Sergo, G. Gubitosa, A. Ferrero and M. Graziani, *J. Catal.*, 1996, **164**, 173.
29 F. H. Chung, *J. Appl. Crystallogr.*, 1974, **7**, 526.
30 A. Trovarelli, F. Zamar, J. Llorca, C. de Leitenburg, G. Dolcetti and J. T. Kiss, *J. Catal.*, 1997, **169**, 490.
31 R. S. Torrens, N. M. Sammes and G. A. Tompsett, *Solid State Ionics*, 1998, **111**, 9.
32 M. Kakihana, S. Kato, M. Yashima and M. Yoshimura, *J. Alloys Compd.*, 1998, **280**, 125.
33 G. Colon, M. Pijolat, F. Valdivieso, H. Vidal, J. Kaspar, E. Finocchio, M. Daturi, C. Binet, J. C. Lavalley, R. T. Baker and S. Bernal, *J. Chem. Soc., Faraday Trans.*, 1998, **94**, 3717.
34 V. G. Keramidas and W. B. White, *J. Am. Ceram. Soc.*, 1974, **57**, 22.
35 M. Yashima, K. Morimoto, N. Ishizawa and M. Yoshimura, *J. Am. Ceram. Soc.*, 1993, **76**, 2865.
36 M. Yashima, K. Arashi, M. Kakihana and M. Yoshimura, *J. Am. Ceram. Soc.*, 1994, **77**, 1067.
37 G. Socrates, *Infrared Characteristic Group Frequencies*, John Wiley & Sons, New York, 1980.
38 M. L. Balmer, F. F. Lange and C. G. Levi, *J. Am. Ceram. Soc.*, 1992, **4**, 946.